Brief Review of Epitaxy and Emission Properties of GaSb and Related Semiconductors

Shouzhu Niu [1] (iD)**, Zhipeng Wei** [1,]*****, Xuan Fang** [1]**, Dengkui Wang** [1]**, Xinwei Wang** [1]**, Xian Gao** [1] **and Rui Chen** [2] (iD)

[1] State Key Laboratory of High Power Semiconductor Lasers, School of Science, Changchun University of Science and Technology, 7089 Wei-Xing Road, Changchun 130022, China; nszcc@outlook.com (S.N.); fangxuan110@126.com (X.F.); wccwss@foxmail.com (D.W.); wxw4122@cust.edu.cn (X.W.); gaoxian1@126.com (X.G.)

[2] Department of Electrical and Electronic Engineering, South University of Science and Technology of China, Shenzhen 518055, China; chen.r@sustc.edu.cn

* Correspondence: zpweicust@126.com; Tel.: +86-158-4309-5977

Abstract: Groups III–V semiconductors have received a great deal of attention because of their potential advantages for use in optoelectronic and electronic applications. Gallium antimonide (GaSb) and GaSb-related semiconductors, which exhibit high carrier mobility and a narrow band gap (0.725 eV at 300 K), have been recognized as suitable candidates for high-performance optoelectronics in the mid-infrared range. However, the performances of the resulting devices are strongly dependent on the structural and emission properties of the materials. Enhancement of the crystal quality, adjustment of the alloy components, and improvement of the emission properties have therefore become the focus of research efforts toward GaSb semiconductors. Molecular beam epitaxy (MBE) is suitable for the large-scale production of GaSb, especially for high crystal quality and beneficial optical properties. We review the recent progress in the epitaxy of GaSb materials, including films and nanostructures composed of GaSb-related alloys and compounds. The emission properties of these materials and their relationships to the alloy components and material structures are also discussed. Specific examples are included to provide insight on the common general physical and optical properties and parameters involved in the synergistic epitaxy processes. In addition, the further directions for the epitaxy of GaSb materials are forecasted.

Keywords: gallium antimonide; alloys and compounds; nanostructures; photoluminescence; molecular beam epitaxy

1. Introduction

The mid-infrared (MIR) spectral region is of great research interest because the practical realization of optoelectronic devices that operate in the 2–5 µm wavelength region would bring potential applications in a wide range of areas, including optical gas sensing, environmental monitoring, free-space optical communications, infrared countermeasures, and thermal imaging [1–3]. Research into MIR semiconductor devices has thus become a focus of research attention worldwide. Groups III–V semiconductors are the most promising candidate infrared materials for use in lasers and detectors, owing to their high absorption coefficients, high carrier mobilities and widely tunable band gaps [1,4]. Among these materials, gallium antimonide (GaSb)-based alloys and compounds offer a wide range of electronic band gaps, band gap offsets and electronic barriers along with extremely high electron mobility; these materials would thus enable a variety of devices that are much faster than the equivalent InP- and GaAs-based devices and infrared light sources, and would

facilitate lower power consumption [5,6]. Therefore, GaSb materials in the forms of epitaxial layers, multi-element alloys, quantum wells, superlattices and low-dimensional nanostructures have been attracting considerable attention. Additionally, based on the GaSb materials described above, a variety of advanced optoelectronic devices, including laser diodes, detectors, and transistors, have been realized [1–4].

Therefore, considerable effort has been devoted to the growth of high-quality GaSb-based semiconductor materials. To date, the growth of GaSb-based semiconductors has mainly been dependent on liquid phase epitaxy (LPE), metal-organic chemical vapor deposition (MOCVD), and molecular beam epitaxy (MBE). MBE is preferred as a high-efficiency epitaxial growth technique that is used to manufacture light-emitting diodes, lasers, and detectors for MIR waveband operation by varying the material components to adjust their energy bands [1,5,7]. By tuning of the growth parameters, a variety of complex quantum structures with high surface and interface quality can be realized. Problems that occur on the GaSb surface during reactive processing, such as high surface state densities, surface Fermi level pinning and a residual native oxide layer, have affected the optical properties, including their photoresponse range and luminescence intensities, of GaSb-based devices. Therefore, procedures that involve the removal of native oxides and the fabrication of passivation coatings are necessary to overcome such problems [8]. Improvements in the surface properties of GaSb materials have led to excellent optoelectronic device performances. As the research into optoelectronic devices has advanced, spectroscopic techniques have become increasingly important because they are highly efficient and rapid modern analysis methods. These techniques can effectively determine the photophysical properties of the materials and reveal their excited-state processes to determine their potential use in optoelectronic devices. Further development of spectroscopic techniques will therefore be helpful in the design and improvement of the next generation of optoelectronic devices. Additionally, two-dimensional (2D) materials offer further promise for the development of a new range of fundamental optoelectronic materials owing to their high crystal quality features and rich photophysical properties that will provide new material options for next generation optoelectronic devices [2,8–10]. Therefore, owing to the advantages of 2D materials, further research should be directed to the epitaxy and optical properties of GaSb materials.

In this paper, we briefly review the literature for the recent progress in the growth and the optical properties of GaSb and GaSb-related materials, and describe the evolution and the current status of epitaxial growth processes and the optical properties of GaSb and related semiconductors. Section 2 provides a brief introduction to some of the epitaxial GaSb materials that have already been grown by the MBE method, Section 3 covers the luminescence mechanism and the spectral characteristics of these materials, along with the factors that influence their optical properties. Section 4 is devoted to the effects of low-dimensional nanostructures on the luminescence properties of these materials. Finally, we discuss GaSb materials fabricated by the MBE method that exhibit unusual optical properties and provide a foundation for the application of these materials in optoelectronic devices.

2. Epitaxy of GaSb Materials

In this review, GaSb and related semiconductors refers to the groups III–V semiconductors that contain the Sb element, including GaAsSb, InAsSb, InGaAsSb and AlGaAsSb. Among these materials, GaSb has a prominent position among the III–V compound semiconductors. GaSb has a lattice constant of 6.0959 Å that mediates between ternary and quaternary III–V compound semiconducting materials (as shown in Figure 1), which enables perfect lattice matching of GaSb to be achieved with many III–V phosphonium-type materials, which is then favorable for high-quality antimony material growth. Additionally, GaSb has a zinc blende (ZB) structure similar to that of GaAs, and its band gap is 0.822 eV at 0 K and 0.725 eV at 300 K [11–13].
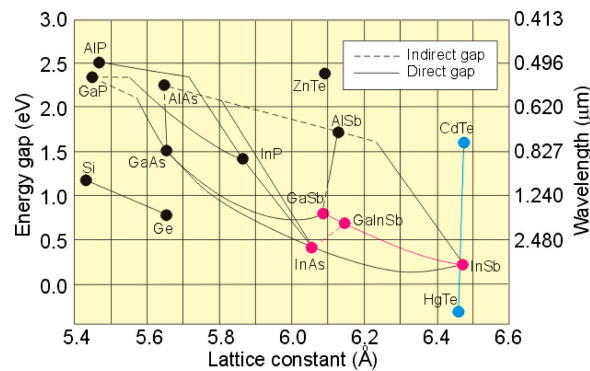
Figure 1. Band gap as a function of lattice constant for III–V compounds and their ternary and quaternary alloys. Reproduced with permission from [11], copyright AIP Publishing LLC (2009).

Liquid phase epitaxy (LPE) was the earliest method used in the extended growth of GaSb-based materials, and there are numerous reports on the growth of GaSb by LPE techniques. In the early studies of the surface morphology and the electrical and optical properties of GaSb layers, it was observed that the growth temperature range of 500–550 °C for the Ga melt is the optimal range to produce high-quality layers with excellent surface morphologies [14]. While epilayers grown at low temperatures have low native defect concentrations, they have poor morphologies and thus are unsuitable for device applications [15]. The typical surface morphologies of GaSb epilayers that were grown at 550 °C from a 660 °C from an Sb-rich melt are as shown in Figure 2. CVD growth of GaSb has been reported by Jakowetzet al. and MOCVD growth of GaSb has also been performed [16,17].
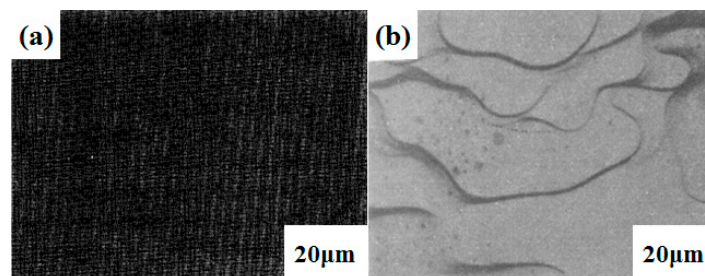

Figure 2. Typical surface morphologies of GaSb epilayers (**a**) grown on a (100) substrate at 550 °C from a Ga-rich melt and (**b**) on a 7° off-axis (111) substrate at 660 °C from an Sb-rich melt. Reproduced with permission from [15], copyright Springer (1995).

At present, antimony is mainly grown using molecular beam epitaxy (MBE) technology, which is based on a nonthermodynamic equilibrium. In recent years, following the development of the nonthermodynamic equilibrium, MBE has been widely used to fabricate a variety of both high-purity single crystals and ultra-fine structures and has thus greatly enhanced the evolution of research into antimony-based materials and devices. MBE is a technique in which single or complex components of an atomic beam or molecular beam are propelled to a heated substrate, are absorbed, migrate, and are deposited on that substrate under ultra-high vacuum conditions [18].

To improve the crystal quality of the epitaxy film, a buffer layer between the epitaxy film and substrate is commonly used, owing to the large difference in lattice constants. InAs, AlSb and GaSb can be used as buffer layers. Noh et al. reported that high quality GaSb films could be realized on a GaAs (001) substrate at low temperature, and the strain relief and structural properties of the GaSb films with different buffer layers were investigated [6]. Their results show that the insertion of an AlSb or GaSb buffer layer is very useful for improving the quality of the GaSb grown on GaAs substrates [6].

As an important part of GaSb materials, multi-component alloys have been intensively investigated. By tuning the components in the alloys, the band gap and lattice constant can be adjusted over a wide range. For example, by theoretical calculations, Wieder and Clawson determined an expression for the band gap of $InAs_xSb_{1-x}$ materials with composition x at temperature T, as follows [19]:

$$E_g(x, T) = 0.441 - \frac{3.4 \times 10^{-4}T^2}{210 + T} - 0.876x + 0.70x^2 + 3.4 \times 10^{-4}xT(1 - x) \tag{1}$$

Among the ternary alloys [20], $GaAs_xSb_{1-x}$ is important owing to the advantage that its wavelength can be modulated over the range from 0.8 µm to 1.7 µm, and such a wavelength band would enable the production of optoelectronic devices with broad application prospects compared with those of InP- and GaAs-based devices. Chou et al. reported on the effects of substrate tilting on the material properties of MBE grown GaAsSb alloys that were closely lattice-matched to InP substrates. GaAsSb alloys with a thickness of 1 µm were grown on InP(100) and off-axis InP substrates (2°, 3° and 4° off-axis) and were characterized by XRD, as shown in Figure 3. Their results are expected to be applicable to devices that incorporate MBE grown GaAsSb in their active layer [21]. However, using Sb as a surfactant would cause a difficulty in epitaxial growth, such as component distribution aggregation. Therefore, the regulation of alloy composition is very important. For this purpose, using a mixed beam, Wei's group reported the carrier dynamics in GaAsSb ternary alloys grown by MBE. The growth conditions and Sb component of the GaAsSb alloy samples were as those shown in Table 1 [22]. The results indicated that the localized states are related to the Sb component of the GaAsSb alloy; however, this component also leads to poor crystal quality in the material, and the applications of GaAsSb alloys are limited owing to the deterioration in quality.
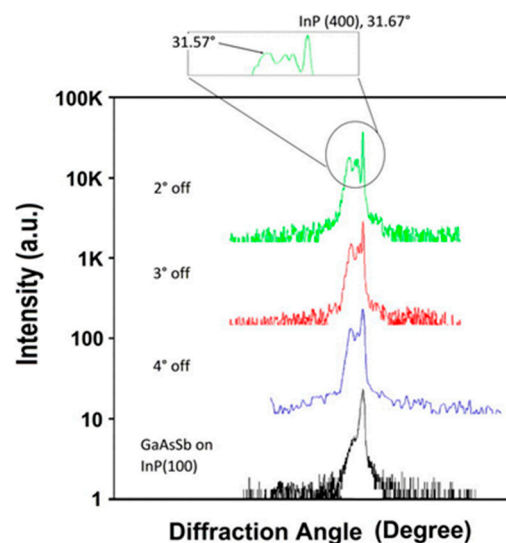

Figure 3. X-ray diffraction (XRD) of 1 µm-thick GaAsSb epi-grown layers on InP (100) and 2°, 3° and 4° off-axis InP (100) substrates. Reproduced with permission from [21], copyright AIP Publishing LLC (2013).

Table 1. Growth conditions of the GaAsSb alloy samples. Reproduced with permission from [22], copyright Nature Publishing Group (2016).

Sample	Growth Temperature	As/Sb Beam Ratio	Sb Component
1		28:1	6%
2	600 °C	16:1	8%
3		7:1	9%

InGaAsSb, which is lattice-matched to GaSb, has been studied in particular depth, in part because it is an important active region constituent of diode lasers emitting in the 2–3 μm range [23]. Early work on the direct band gap in GaSb-rich GaInAsSb has been summarized by Karouta et al., who proposed a bowing parameter of 0.6 eV [24]. In a recent report, an absorption layer composition of $In_{0.28}Ga_{0.72}As_{0.25}Sb_{0.75}$ allowed for lattice matching to GaSb and demonstrated cut-off wavelengths of 2.9 μm at 250 K and 3.0 μm at room temperature [25]. Figure 4 shows the photoluminescence results recorded between 4 and 300 K. Additionally, short-wave infrared barriode detectors can be realized.
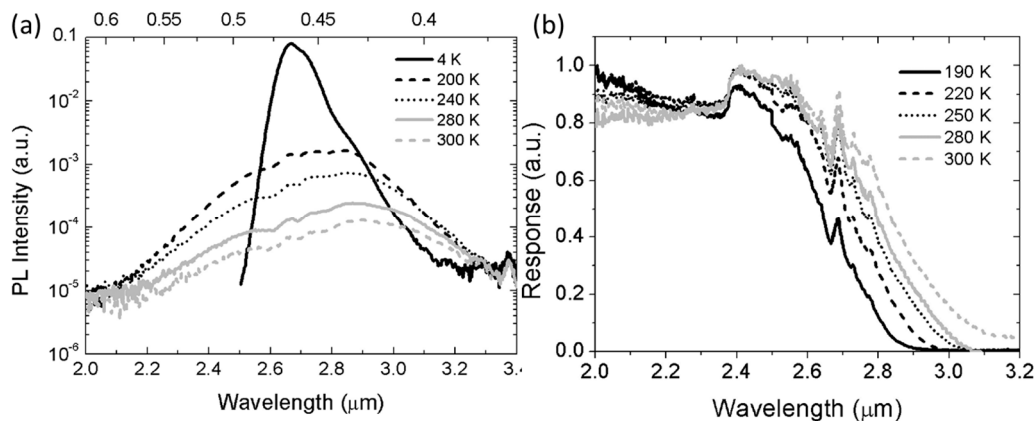

Figure 4. (**a**) Photoluminescence results measured between 4 and 300 K and (**b**) normalized spectral response data between 190 and 300 K. Reproduced with permission from [25], copyright AIP Publishing LLC (2015).

In a similar way to InGaAsSb, AlGaAsSb is also important, as it is lattice-matched to GaSb and forms a natural barrier and cladding material for use in mid-infrared semiconductor lasers. The relationships for the direct and indirect energy gaps were calculated by Adachi and the experimental results were summarized by Ait-Kaci et al. [26,27]. An accurate determination of the chemical composition of AlGaAsSb layers is difficult. Figure 5 shows the band-gap energies as a function of the *x*-composition parameter for $Al_xGa_{1-x}As_ySb_{1-y}$ when it is lattice-matched to GaSb.
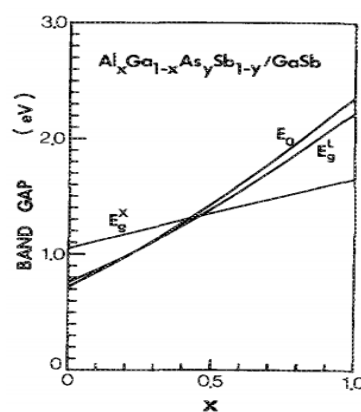

Figure 5. Band-gap energies as a function of the *x*-composition parameter for $Al_xGa_{1-x}As_ySb_{1-y}$ when lattice matched to GaSb. Reproduced with permission from [26], copyright AIP Publishing LLC (1987).

In a recent study, Jasik et al. reported on their investigation of the composition of MBE-grown AlGaAsSb layers in the context of unintentional arsenic incorporation. Based on the results obtained, a procedure for the determination of the chemical composition of AlGaAsSb materials was proposed. Table 2 lists the chemical compositions of multicomponent layers [28].

Table 2. Chemical compositions of multicomponent layers. (Reproduced with permission from Jasik et al., Journal of Applied Physics; published by the American Institute of Physics, 2011 [28]).

Sample	Relaxation Degree (%)	Stoichiometry Coefficient x	y	Lattice Constant (Å)	Lattice Mismatch (ppm), Relaxed	Lattice Mismatch (ppm),$(\sin\theta_s / \sin\theta_L) - 1$
#A01T	45	0.430	–	6.11255	2814	2837
#A02T	10	0.355	–	6.10956	2324	4267
#A03T	44	0.480	–	6.11455	3142	4782
#A01Q	0	0.430	0.0437	6.09277	−431	−820
#A02Q	10	0.355	0.0045	6.10753	1989	3664
#A03Q	0	0.480	0.0319	6.09997	750	1463

3. Optical and Emission Properties of GaSb Materials

Optical properties have also been intensely investigated as a standard for evaluating material quality and device performance. At present, GaSb materials are believed to have potential for optoelectronic applications. To exploit the full potential of these materials for structural design, a clear understanding of the properties of the material system, e.g., the band parameters and carrier dynamics, is required. Photoluminescence (PL) is a type of spontaneous emission in which light is emitted from a material. The peak energy and intensity of PL are mostly dependent on the regions in the materials that are excited. Basically, PL measurement is a useful tool for the characterization of material parameters and is helpful for understanding the dynamic carrier processes in materials [29]. For example, PL measurements are advantageous in studies of optical emission processes, material composition, and impurity content. To give an overview of the optical properties of GaSb materials, we will first review the previous work in this field over recent decades.

3.1. GaSb Emission Properties

Undoped GaSb is a direct band gap semiconductor with a gap of approximately 0.8 eV, which is always p-type. In 1997, Dutta et al. presented a comprehensive review of GaSb growth technology, including the resulting structural, electronic and transport properties, along with a few optical properties [11]. In this section, we will provide a brief review of the PL properties of GaSb materials.

The luminescence properties of undoped p-GaSb were studied as early as 1972 by Jakowetz et al., who observed that a doubly-ionizable acceptor affected the concentration of holes in undoped GaSb [16]. Figure 6 shows the experimental PL data for undoped GaSb. The peak emission at 810 meV was attributed to a free exciton, and the emission line at 795.5 meV was identified as arising from to a bound exciton [30]. The lines A, B and C were interpreted as transitions from the conduction band to the three acceptor levels. The acceptor ionization energies denoted by EA, EB and EC were 34.5, 55 and 102 meV, respectively [16,31–33]. The energy positions and corresponding interpretations are listed in Table 3. Jakowetz et al. concluded that the simplest possible model for the acceptor is that of an antistructure defect, that is, as a Ga atom on an Sb site. However, they also admitted that it may possible for more complex defect structures in undoped GaSb to exist. According to the work of Lee et al., unintentionally doped GaSb can display approximately 20 transitions in the 680–810 meV range in the low temperature PL spectra. While a few of these transitions have clear associations with specific defects, the PL measurements offer great advantages for further research. The PL properties can be very different when using a specific growth method or specific growth conditions. For samples grown using MBE technology, better crystallinity is obtained when using a growth temperature range of 500–550 °C and an Sb_4:Ga flux ratio of more than 1.5 [34]. In another study, buffer layers were used to reduce the defect concentrations [35]. Clearly, high-quality MBE-grown GaSb, which demonstrates higher carrier mobility, can be obtained by the optimization of the growth conditions [33–36]. More importantly, PL measurements can serve to determine the transitions that occur in good quality GaSb materials [33]. First, the free exciton (FE) transition is an indication of high optical quality. However, several bound excitonic transitions (BE_1–BE_4) are generally

observed and tend to dominate the emissions from MBE-grown samples. These acceptor-related transitions are listed in Table 4. Additionally, the transition energy may be caused by a concentration of unintentionally incorporated donors, strain effects, or competing free-to-bound and donor-acceptor transitions. More recently, researchers found that the free electron to hole bound to unidentified acceptor transition could dominate recombination after Te doping of GaSb, particularly at high doping levels [36]. Since then, the PL properties caused by doping effects have attracted scientific and technological interest motivated by optoelectronic device design considerations [37]. As the growth techniques matured, the next challenge was to fabricate ternary and quaternary alloys to meet the requirements of heterostructure fabrication.
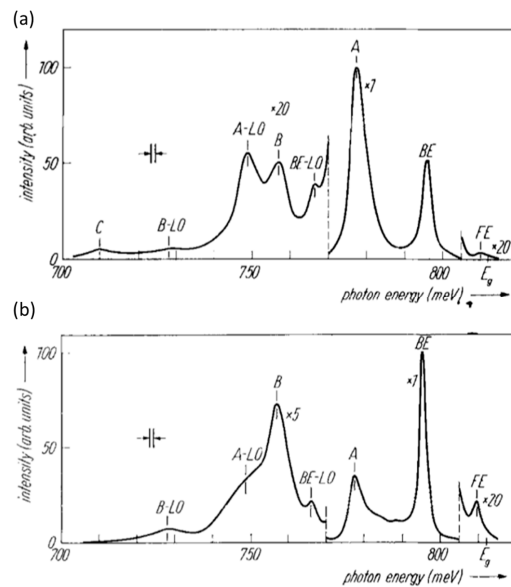

Figure 6. Experimental photoluminescence (PL) data for undoped GaSb. (**a**) PL spectrum of GaSb sample W4, grown from a stoichiometric melt. $p_{300} = 1.8 \times 10^{17}$ cm^{-8}, T = 2 K; (**b**) PL spectrum of GaSb sample W7, grown from an antimony rich melt. $p_{300} = 3.5 \times 10^{16}$ cm^{-3}, T = 2 K; Reproduced with permission from [16], copyright Wiley-VCH (1972).

Table 3. Energetic positions and corresponding interpretations for GaSb. Reproduced with permission from Jakowetz et al., Physica Status Solidi; published by the Weinheim, Germany: Wiley-VCH, 1972 [16].

Line	hυ (mev)	
FE	810	free exciton
BE	795.5	bound exciton
A	777.5	band-acceptor transition $E_A = 34.5$ meV
BE-LO	766	phonon replica of line BE $(LO)_\Gamma$-phonon: $(hυ)_{Ph} = 29.5$ meV
B	757	band-acceptor transition $E_B = 55$ meV
A-LO	748.5	phonon replica of line A $(LO)_\Gamma$-phonon: $(hυ)_{Ph} = 29$ meV
B-LO	728	phonon replica of line B $(LO)_\Gamma$-phonon: $(hυ)_{Ph} = 29$ meV
C	710	band-acceptor transition $E_c = 102$ meV second ionization step of the acceptor involved in line A
D	803	band-acceptor transition? $E_D = 9$ meV

Table 4. Acceptor-related transitions of GaSb. Reproduced with permission from Lee et al., Journal of Applied Physics; published by the American Institute of Physics, 1986 [33].

Energy (meV)	FWHM (meV)	Notation
806	3	BE1
802	2	BE2 or BE3
800–790	Unresolved	BE4 and other acceptor related transitions
785	10–15	Unidentified acceptor U_1
775	5	
757	Unresolved	
746	7–8	A_{LO} Phonon replica
725	10	
722	Unresolved	U_2
717	2–3	U_3
710	5	U_4

3.2. GaSb Alloy Emission Properties

From the previous section, owing to band tailoring properties of GaAsSb being important for devices with hetero-epitaxial structural designs, and particularly edge-emitting lasers [35,38] and vertical cavity surface-emitting lasers (VCSELs), many research efforts have been made in epitaxy growth of GaSb materials. In recent decades, MBE growth of $GaAs_{1-x}Sb_x$ over the entire composition range has been reported [39,40], and ternary compounds have been estimated using Vegard's law [41]. The relationship between the composition and the band gap energy can be expressed as [42]

$$E_g = 1.43 - 1.9x + 1.2x^2 \tag{2}$$

However, with the component distribution aggregation effect, the optical properties would exhibit a distinct phenomenon, such as emission related to localized states [22]. Unfortunately, there have only been a few reports on the optical properties of GaAsSb materials [43–50]. In addition, GaAsSb has been recognized as an important material for use in high-performance optoelectronic devices, and its optical properties are thus significant for the improvement of the performance of these devices. Basic knowledge of the properties of GaAsSb is thus important for further applications of the material. Specifically, the incorporation of small fractions of antimony (Sb) in GaAsSb materials leads to the reduction of the band gap and introduces some localized states that are caused by fluctuations in the Sb content.

The $GaAs_xSb_{1-x}$ transition process is an important advantage of the material when used in potential band engineering applications, particularly in the research on $GaAs_xSb_{1-x}$ grown by MBE technology. Hsu et al. presented an optical study of low-Sb-component $GaAs_xSb_{1-x}$ layers and identified the conduction to heavy-hole (HH) band and conduction to light-hole (LH) band transitions that were determined to originate from strain-induced valence band splitting by comparing the relative intensities of the photoreflectance (PR) and piezoreflectance (PzR) spectra [48]. The splitting behavior of the valence band relative to the Sb content is shown in Figure 7. Qiu et al. studied the optical spin polarization properties of $GaAs_{0.94}Sb_{0.06}$ to demonstrate how Sb incorporation modified the spin properties of GaAs [49]. Gao et al. focused on the carrier dynamics of $GaAs_xSb_{1-x}$ epilayers with low Sb content [22]. They discovered the phenomenon of carrier localization, and the degree of localization showed a linear relationship with increasing Sb content. These localized states were related to the Sb component in $GaAs_xSb_{1-x}$, and could lead to optical emission degeneration (as shown in Figure 8.).
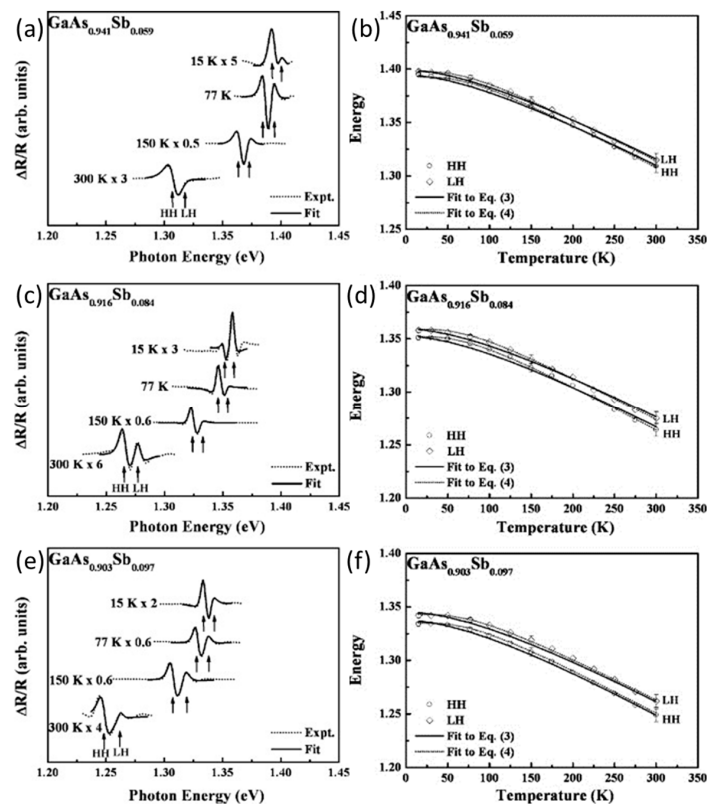
Figure 7. Valence band splitting behavior with respect to the Sb content of GaAs$_x$Sb$_{1-x}$. PR spectra (dotted curves) of GaAs$_{1-x}$Sb$_x$ samples for (**a**) Sb = 5.9%, (**c**) Sb = 8.4% and (**e**) Sb = 9.7% at 15, 77, 150, and 300 K. The full lines are least-squares fits to FDLL; Temperature variations of the experimental PR values for HH and LH transition with representative error bars for GaAs$_{1-x}$Sb$_x$ with (**b**) Sb = 5.9%, (**d**) Sb = 8.4%, and (**f**) Sb = 9.7% as open-circles and open-diamonds, respectively. The obtained values of the transition energies are indicated by the arrows. Reproduced with permission from [48], copyright Elsevier S. A. (2010).
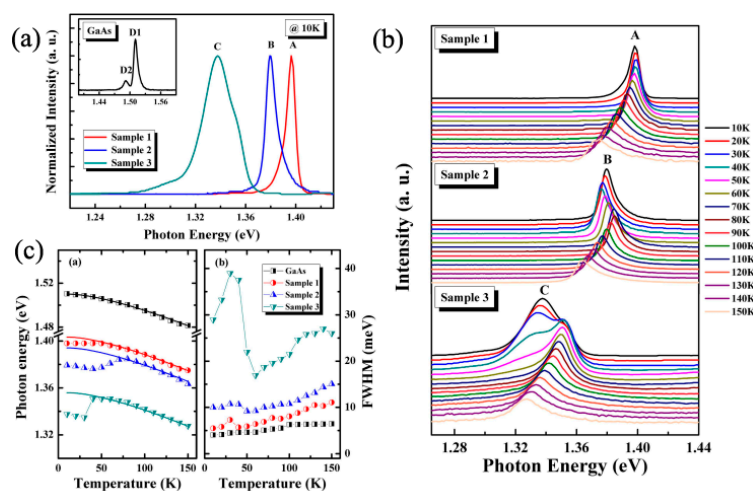
Figure 8. (**a**) PL spectra of GaAs$_x$Sb$_{1-x}$ alloy samples at 10 K; the inset shows the PL spectrum of GaAs substrate at 10 K, (**b**) temperature-dependent PL characteristics of GaAsSb, and (**c**) (i) temperature dependent peak position and (ii) temperature dependent FWHM of the samples. Reproduced with permission from [22], copyright Nature Publishing Group (2016).

The localized states may be generated by the composition fluctuation, which should therefore be suppressed to optimize the optical properties of the material. However, post annealing treatment has been commonly used to improve the structural and optical properties quality of semiconductors, and can be used to reduce the localized states occurring in GaAs$_x$Sb$_{1-x}$ layers. It should be noted that the formation of localized states was related to Sb cluster formation inside the GaAs$_x$Sb$_{1-x}$ alloy, which was influenced by the rapid thermal annealing (RTA) temperature. Figure 9 shows the effects of the RTA temperature on the emission properties [50]. During the RTA process, a significant change in the PL, owing to the reduction of localized states, was observed. The distribution of the composition in GaAs$_x$Sb$_{1-x}$ resulting from the annealing can cause a slight red-shift of the maximum photoluminescence peak. More important, the RTA process can induce Sb migration and a fluctuation in alloy composition; therefore, the optimal RTA temperature should be used to improve the optical properties of the GaAs$_x$Sb$_{1-x}$ alloy material.
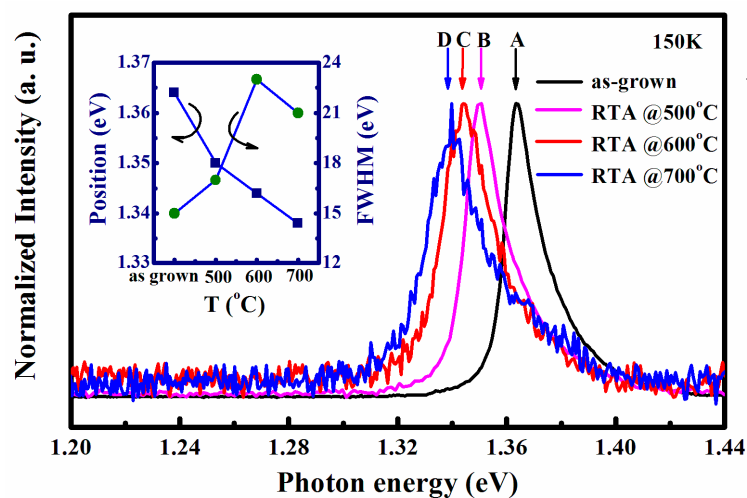

Figure 9. Effects of rapid thermal annealing (RTA) temperature on the emission properties of GaAs$_x$Sb$_{1-x}$. Reproduced with permission from Gao et al., Optical Materials Express; published by the Optical Society of America, 2017 [50].

3.3. Effects of Surface States on GaSb Materials

The superficial and interfacial characteristics can affect the performance of semiconductor devices. The surfaces of GaSb materials can oxidize rapidly in the atmosphere because of their highly reactive chemical properties, and the performance of devices based on these materials is largely dependent on the properties of the surfaces or interfaces. The development of GaSb-based devices could thus easily be hampered by the surface properties of the material. Generally, these surface states can lead to the poor photoelectric efficiency of optoelectronic devices. Specifically, an oxide layer forms during the oxidation process and an undesirable conduction path arises at the oxide/GaSb-based material interface because of the elemental Sb content [51]. Surface states are induced by these native oxides and can cause high surface recombination velocities and large leakage currents [52–55]. With the intent to improve these surface properties, various chemical treatments have been used to reduce the surface states in GaSb materials and thus improve the properties of the materials. In particular, the sulfuration technique (a surface treatment using a sulfur-containing solution) is showing potential to improve the density of surface states for surface passivation of III–V compounds. A number of works have focused on the use of models to describe the sulfur passivation process. One of the most widely accepted models can be expressed using the following form [54]:

$$A^{III}B^V + HS^- + H_2O \rightarrow \left(A^{III}\right)_{X'} S_y + \left(B^V\right)_{X'} S_y + OH^- + H_2 \uparrow \qquad (3)$$
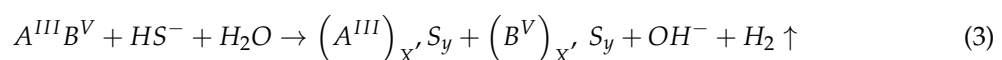
The sulfur passivation process can be described using the schematic diagram shown in Figure 10. The first stage involves breaking the bonds between the A^{III} and B^{V-} atoms (as shown in Figure 10a). Next, the chemical bonds are released to enable the formation of S-A^{III} and/or S-B^{V} (as shown in Figure 10b). Then, chemical bonds are formed between sulfur and the other atoms on the semiconductor surface (as shown in Figure 10c,d). We therefore present some examples to introduce the wet method used for the sulfur passivation process.
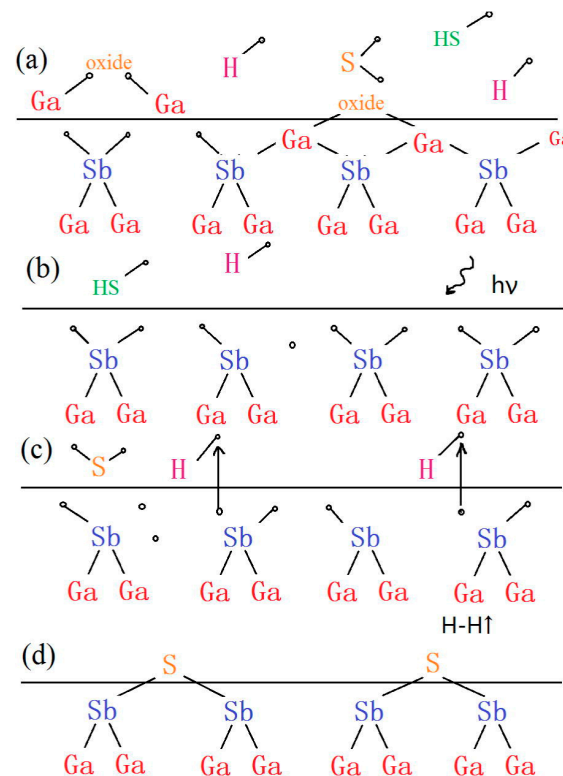
Figure 10. Schematic showing the chemical bonds between sulfur and other atoms formed at the semiconductor surface. Reproduced with permission from [8], copyright NORTH-HOLLAND (2013).

Wet methods of sulfur passivation based on the use of sulfur solutions have been proved to effectively reduce the surface states. For example, $(NH_4)_2S$ and Na_2S solutions are usually used to passivate GaSb surfaces [8]. Figure 11 presents the passivation time-dependent emission intensities of GaSb samples. The PL results indicate that the emission intensity of the passivated GaSb sample could be raised to be 15 times higher than that of the as-grown samples. From low temperature PL measurements, the reason for the enhanced emission intensity was determined to originate from the enhancement of free exciton emission. This wet method of sulfur passivation of GaSb-based materials is thus demonstrated to be promising for the development of efficient light-emitting materials, which means the application of GaSb materials in potential optoelectronic device is feasible [55].
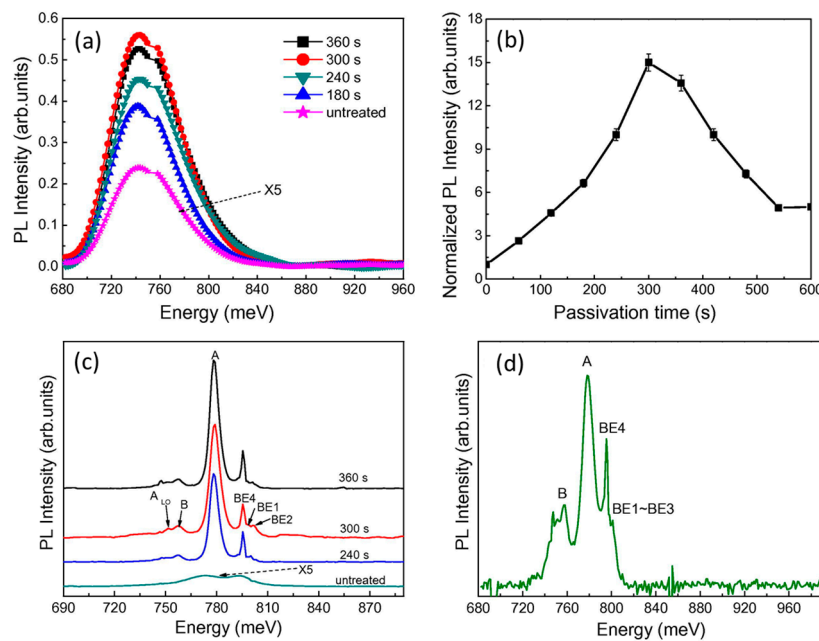
Figure 11. Passivation time dependence of the emission intensity of the GaSb samples, (**a,b**) shows the PL spectra of the untreated GaSb and the passivated GaSb in $(NH_4)_2S$ solution for different passivation times, (**c**) shows the low temperature PL spectra of GaSb and passivated GaSb, (**d**) logarithmic PL spectrum of GaSb sample at 10 K. Reproduced with permission from [8], copyright NORTH-HOLLAND (2013).

4. Low-Dimensional Nanostructures of GaSb Materials

The nanowire (NW) with its one-dimensional (1D) structure is the smallest structure that can be used for the efficient transport of electrons and optical excitation; NWs are thus expected to be critical to the functionality and integration of nanoscale devices [56–59]. Among these structures, because of their outstanding potential for use in the fabrication of high-performance nano-optoelectronic devices, III–V semiconductor NWs have attracted considerable research attention. For laser applications, the NW provides two of the required components for lasing, that is, the gain medium and the cavity, and thus is a suitable material for use in photonic laser applications [60]. Recently, lasing has been realized at room temperature in core-shell GaAs/AlGaAs NWs [61]. Simultaneously, because the NW has the obvious virtues of light absorption and carrier collection, it has also been the focus of research for the development of the next generation of photovoltaic materials. Krogstrup et al. reported that a solar cell made from NWs can even break the Shockley-Queisser limit [62]. In addition, III–V NWs have been widely studied for use in detectors, single-photon sources and transistors [63–65].

As a result of the narrow bang gap and high electron mobilities, GaSb NWs can offer significant advantages in the mid-infrared range, especially for ~2 μm. Consequently, there has been considerable interest in research into GaSb NWs for nanodevice applications [66–69]. Yang et al. reported the growth of GaSb nanowires on Si substrates using CVD. However, these GaSb NWs were coil-like and became intertwined, which made device fabrication difficult [70]. A. H. Chin used GaSb subwavelength wires with a cross-sectional dimension of 700–1500 nm and lengths of 10–70 μm to lase at approximately 1550 nm, as shown in Figure 12 [71]. Additionally, the higher carrier concentrations mean that these NWs also contain large numbers of native crystal defects. Clearly, there is a need for a more robust method for the preparation of GaSb NWs.
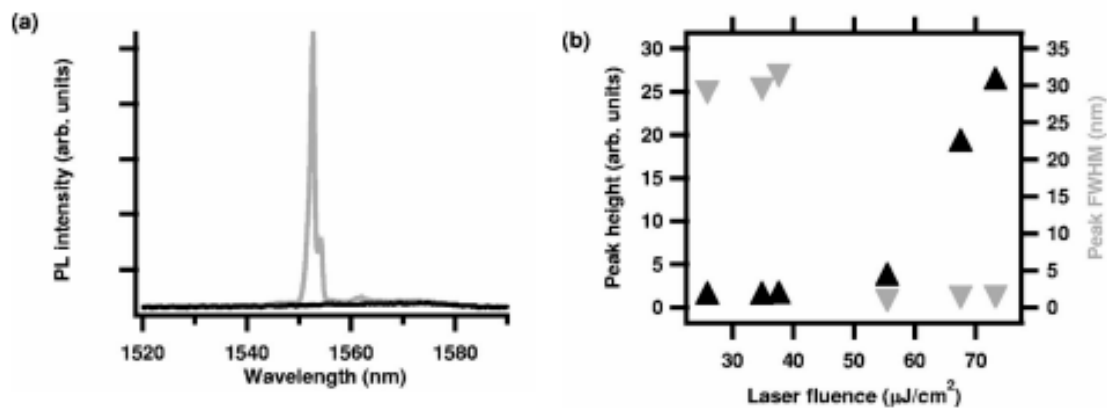
Figure 12. GaSb semiconductor subwavelength wires (SWW) NIR lasing, (**a**) PL spectra below (black) and well above threshold (gray), (**b**) Peak PL height at the lasing line wavelength of 1553 nm (black, up triangles) and PL width (gray, down triangles) vs laser fluence. Reproduced with permission from [71], copyright AIP Publishing LLC (2006).

MBE is a feasible method to grow GaSb NWs which has been used to produce a number of different III–V NWs, including GaN, GaAs, InAs and InSb structures [72–74]. In MBE, the vapor–liquid–solid (VLS) mechanism is the most extensively used growth mechanism. This mechanism is dependent on the liquid metal catalyst. During the growth process, the group III and group V elements are dissolved in the catalyst and the catalyst-substrate interface reaches supersaturation. More supersaturated elements are precipitated out and this leads to the NW growth. This process is influenced by the substrate, the growth temperature, the catalyst, the V/III flux ratio and the flux types used [75–78]. These factors thus jointly affect the physical dimensions and the crystal quality of the resulting NWs. It should be noted that the NWs show two typical crystal structures: the zinc blend (ZB) and wurtzite (WZ) crystal structures (as shown Figure 13), which are difficult to achieve in thin film growth [79]. Therefore, crystal structure control technology for NW fabrication has become a focus of the current research.
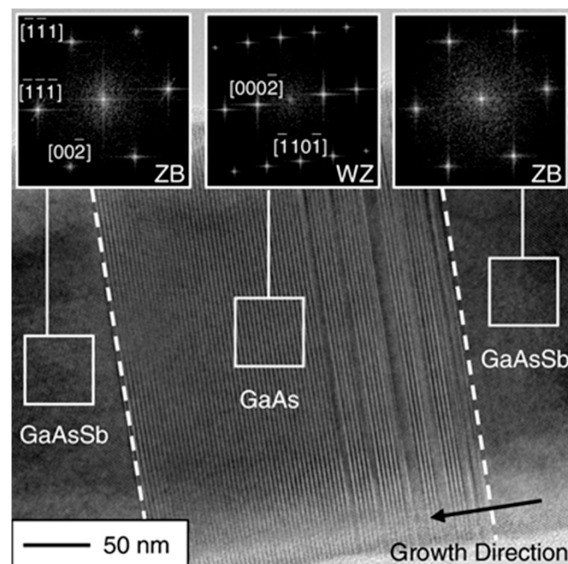

Figure 13. HRTEM image of the GaAsSb/GaAs/GaAsSb heterostructure with the zinc blend and wurtzite crystal structures. Reproduced with permission from [79], copyright AIP Publishing LLC (2010).

While MBE is widely used to grow III–V NWs, many problems remain to be solved for the growth of GaSb-based NWs. However, the fabrication of GaSb-based NWs is thus a core challenge. When compared with other group V elements, the saturated vapor pressure of Sb is higher and this makes the growth of these NWs much more difficult. In the III–Sb NW formation process, the Sb suppresses Ga diffusion and reduces the contact angle of the catalyst [80]. All these factors mean that GaSb can easily form thin films but NW formation is much more difficult. Recently, MBE growth of Ga-catalyzed GaSb NWs was realized on a GaAs stem (as shown Figure 14). Research into this growth method has just started and further investigation is required [81].
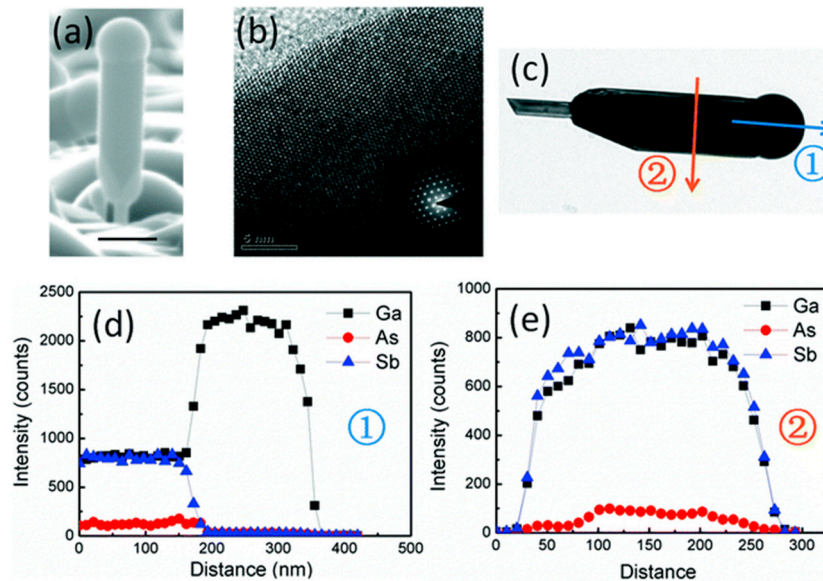

Figure 14. (**a**) A typical SEM image of the GaSb section (**b**) High resolution TEM of a GaSb nanowire (NW). The inset is the SAED image from the same GaSb NW. (**c**) TEM image of a GaSb section showing the directions of EDX line scans. (**d,e**) are the corresponding EDX line scans along the axial and cross-axial directions, respectively. Reproduced with permission from [81], copyright RSC Pub (2016).

To control the photoelectric characteristics of NWs, other III–V elements have been introduced into GaSb NWs to form ternary nanowires, such as GaAsSb, InAsSb, GaAsP, and GaInSb NWs [82–84]. Among these structures, the GaAsSb NWs are one of the most frequently researched structures. GaAsSb NWs fabricated by MBE can be divided into two types: those grown on Si(111) substrates and those grown on GaAs nanowire stems. The GaAsSb NWs have been realized with Sb components in the 0–0.44 range [85–87]. This makes the band gap of GaAsSb NWs easier to be tuned. By growth of the AlGaAs passive layer, Dingding Ren et al. realized for the first time the wavelength tunability of the optical emission from self-catalyzed GaAsSb nanowire arrays, and a tuning range from 1.219 to 1.422 eV [80]. Recently, by tuning of the background As, Li et al. realized near-full composition range GaAsSb NWs (GaAs$_{1-x}$Sb$_x$ nanowires with x ranging from 0.60 to 0.93), and the emission wavelength of these GaAsSb NWs was tunable from 844 nm to 1760 nm [5]. Moreover, Dheeraj et al. demonstrated for GaAs NWs with GaAsSb inserted, the band alignment was a staggered type II (as shown Figure 15) [88]. The electrons and holes were confined in the GaAs layers and GaAsSb layers separately. The emission wavelength changed when the band offset of GaAs/GaAsSb was changed. This provides a new way to control the emission wavelength of NWs.
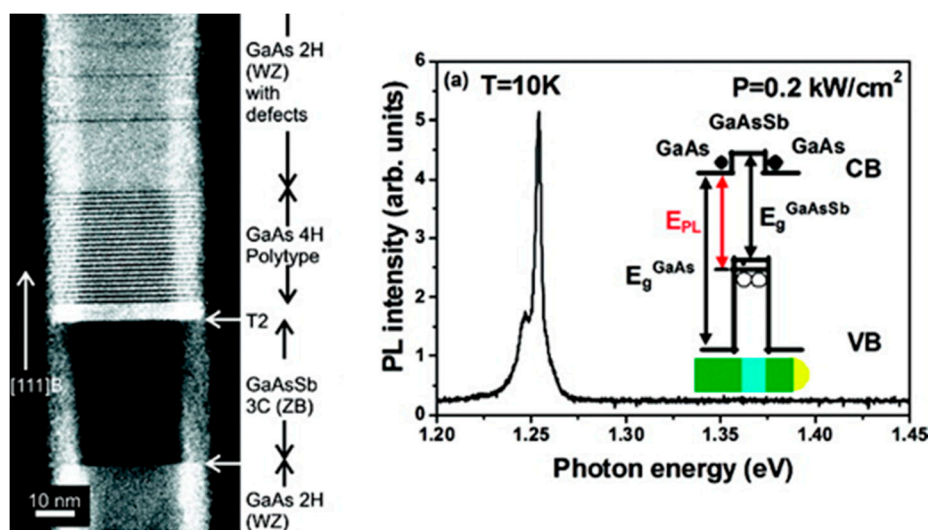
Figure 15. (**a**) TEM images of the GaAs/GaAsSb NWs and (**b**) low temperature PL spectrum of a single GaAs/GaAsSb NW. Reproduced with permission from [88], copyright American Chemical Society (2010).

The crystal structure is another focus of research in this field. Ren et al. demonstrated Sb-induced effects on the crystal structures of self-catalyzed GaAsSb NWs [80]. By increasing the Sb content, a WZ phase GaAsSb NW can be changed into a ZB GaAsSb NW (as shown Figure 16). Conesa-Boj et al. demonstrated large area vertical GaAsSb nanowire arrays [89]. The nanowires exhibited a pure zinc blende crystal structure and were entirely twin-free down to the first bilayer, which provides a foundation for the production of a high-quality NWs device.
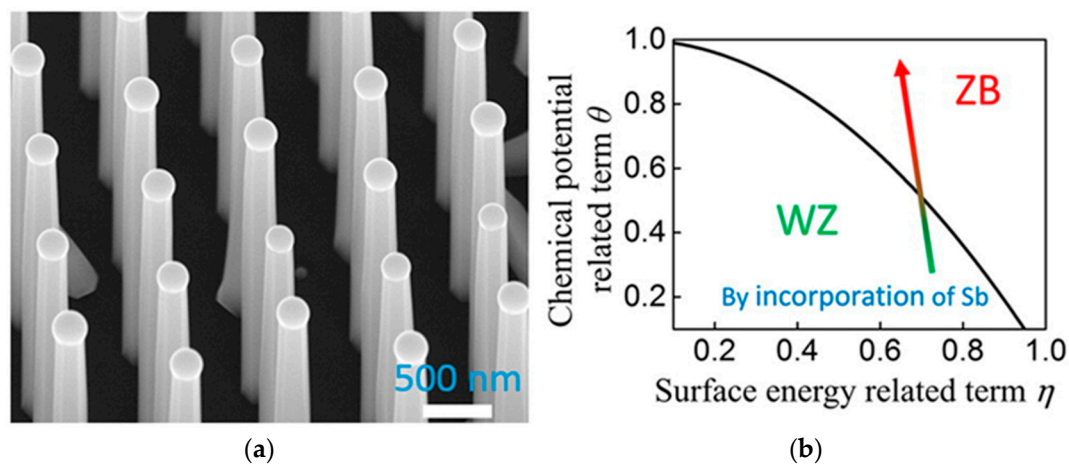

(**a**)　　　　　　　　　　　　　　　　　　　　　(**b**)

Figure 16. (**a**) SEM images of GaAsSb NW arrays and (**b**) WZ-ZB crystal phase diagram for catalyst-assisted NW growth. The solid lines show the WZ-ZB nanowire crystal phase-equilibriumlines with respect to η and θ. The labeled arrows represent how the crystal phase diagrams correlate with different crystal phase control strategies. Reproduced with permission from [80], copyright American Chemical Society (2016).

When compared with GaAs and InAs NWs, the research into GaSb and related alloy nanowires is still insufficient. Current studies are focused on the preparation of the NWs, and there are many challenges to be overcome. Therefore, more research is needed on antimony-based NW growth and characteristics.

5. Conclusions

Over the past few decades, many III–V semiconductor materials and devices have been grown using molecular beam epitaxy (MBE) methods [90–93]. The properties of antimonide materials have been studied intensively. Infrared lasers and detectors based on MBE-grown materials have been widely investigated, and their performances have been adequate for their intended applications [94,95]. The variable temperature PL properties of antimonide films and nanostructures have also been reported, and the origins of the PL peaks have been determined. The PL of antimonide alloys is usually dominated by surface states, bound carrier recombination and vacancy defect-related emissions [96,97]. Surface passivation can improve the optical properties of these materials because it eliminates surface dangling bonds and oxides [8]. Low-dimensional antimonide alloy structures were then grown as the MBE technology matured. The controllable growth of GaSb-based NWs has already been realized by some research groups [98]. The optical properties of NWs are similar to those of thin films, but the surface states in NWs are comparatively enormous; this can be attributed to their high surface-to-volume ratios. Establishing the relationship between the growth conditions and the optical properties of these structures is highly significant for the investigations of low-dimensional structures. On this basis, the research efforts into one-dimensional semiconductor devices remain ongoing and are still in their initial stages.

While GaSb-based ternary and quaternary alloys have also been grown by MBE, other multicomponent alloys, such as quinary alloys, must be studied for practical applications. Component segregation, aggregation and diffusion processes are more likely to occur in quinary alloys; this has great value for component control research. For one-dimensional GaSb materials, it is also necessary to control the component ratio. While the optical properties of alloy NWs have been reported by several groups, a further comprehensive study of the relationships among the surface states, the defects and the emission spectra is required. Additionally, improvement of the optical properties of these materials is also an important research direction. New methods should be developed in addition to surface passivation. Meanwhile, besides the above-mentioned research direction, with the lattice and coefficient of thermal expansion ability, GaSb is a desirable substrate candidate for epitaxial growth of mid-wave infrared (MWIR) materials and devices, such as HgCdTe on GaSb. The results indicate that the lattice misorientation/misfit dislocations in HgCdTe could be greatly suppressed by using a GaSb substrate [99–101]. Therefore, it is widely considered that MBE growth of HgCdTe on GaSb substrates should be important for application in next generation infrared detectors.

As we know, two-dimensional or layered materials may also offer remarkable optical performances, showing potential applications in a range of fields including hydrogen evolution, transistors and optoelectronic devices [102,103]. To date, two-dimensional GaN has been grown by a migration-enhanced encapsulated growth technique that uses epitaxial graphene [104]. Additionally, As- and Sb-based two-dimensional materials, called arsenene and antimonene, respectively, have been synthesized [105]. Although 2D materials based on GaSb have not been realized, many experts have already carried out the theoretical research of GaSb two-dimensional structures [106–108]. Therefore, GaSb 2D materials should also be realized in the future and represent another important research direction. While there have been no reports of two-dimensional GaSb structures to date, major research efforts should be made in this area.

References

1. Borg, B.M.; Wernersson, L.E. Synthesis and properties of antimonide nanowires. *Nanotechnology* **2013**, *24*, 202001. [CrossRef] [PubMed]

2. Cui, Q.; Yang, Y.; Li, J.; Teng, F.; Wang, X. Material and device architecture engineering toward high performance two-dimensional (2D) photodetectors. *Crystals* **2017**, *7*, 149. [CrossRef]

3. Chen, H.; Liu, H.; Zhang, Z.; Hu, K.; Fang, X. Nanostructured photodetectors: From ultraviolet to terahertz. *Adv. Mater.* **2016**, *28*, 403–433. [CrossRef] [PubMed]

4. Zhang, Y.; Wu, J.; Aagesen, M.; Liu, H. III–V nanowires and nanowire optoelectronic devices. *J. Phys. D Appl. Phys.* **2015**, *48*, 463001. [CrossRef]

5. Li, L.; Pan, D.; Xue, Y.; Wang, X.; Lin, M.; Su, D.; Zhang, Q.; Yu, X.; So, H.; Wei, D. Near full-composition-range high-quality $GaAs_{1-x}Sb_x$ nanowires grown by molecular-beam epitaxy. *Nano Lett.* **2017**, *17*, 622–630. [CrossRef] [PubMed]

6. Noh, Y.; Hwang, Y.; Kim, M.; Kwon, Y.; Oh, J.; Kim, Y.; Lee, J. Structural properties of GaSb layers grown on InAs, AlSb, and GaSb buffer layers on GaAs (001) substrates. *J. Korean Phys. Soc.* **2007**, *50*, 1929. [CrossRef]

7. LaPierre, R.; Robson, M.; Azizur-Rahman, K.; Kuyanov, P. A review of III–V nanowire infrared photodetectors and sensors. *J. Phys. D Appl. Phys.* **2017**, *50*, 123001. [CrossRef]

8. Wang, B.; Wei, Z.; Li, M.; Liu, G.; Zou, Y.; Xing, G.; Tan, T.T.; Li, S.; Chu, X.; Fang, F. Tailoring the photoluminescence characteristics of p-type GaSb: The role of surface chemical passivation. *Chem. Phys. Lett.* **2013**, *556*, 182–187. [CrossRef]

9. Solís-Fernández, P.; Bissett, M.; Ago, H. Synthesis, structure and applications of graphene-based 2D heterostructures. *Chem. Soc. Rev.* **2017**, *46*, 4572–4613. [CrossRef] [PubMed]

10. Ji, J.; Song, X.; Liu, J.; Yan, Z.; Huo, C.; Zhang, S.; Su, M.; Liao, L.; Wang, W.; Ni, Z. Two-dimensional antimonene single crystals grown by van der Waals epitaxy. *Nat. Commun.* **2016**, *7*, 13352. [CrossRef] [PubMed]

11. Rogalski, A.; Antoszewski, J.; Faraone, L. Third-generation infrared photodetector arrays. *J. Appl. Phys.* **2009**, *091101*. [CrossRef]

12. Johnson, G.; Cavenett, B.; Kerr, T.; Kirby, P.; Wood, C. Optical, Hall and cyclotron resonance measurements of GaSb grown by molecular beam epitaxy. *Sermicond. Sci. Technol.* **1988**, *3*, 1157. [CrossRef]

13. Vurgaftman, I.; Meyer, J.R.; Ram-Mohan, L.R. Band parameters for III–V compound semiconductors and their alloys. *J. Appl. Phys.* **2001**, *89*, 5815–5875. [CrossRef]

14. Dutta, P.; Rao, K.K.; Bhat, H.; Naik, K.G.; Kumar, V. Surface morphology, electrical and optical properties of gallium antimonide layers grown by liquid phase epitaxy. *J. Cryst. Growth* **1995**, *152*, 14–20. [CrossRef]

15. Dutta, P.S.; Bhat, H.L.; Kumar, V. Liquid phase epitaxial growth of pure and doped GaSb layers: Morphological evolution and native defects. *Bull. Mater. Sci.* **1995**, *18*, 865–874. [CrossRef]

16. Jakowetz, W.; Rühle, W.; Breuninger, K.; Pilkuhn, M. Luminescence and photoconductivity of undoped p-GaSb. *Phys. Stat. Sol.* **1972**, *12*, 169–174. [CrossRef]

17. Shin, J.; Verma, A.; Stringfellow, G.; Gedridge, R. Growth of GaSb using trisdimethylaminoantimony. *J. Cryst. Growth* **1995**, *151*, 1–8. [CrossRef]

18. Parker, E.H.C. Silicon Molecular beam epitaxy. In *Molecular Beam Epitaxy and Heterostructures*; Leroy, L.C., Klaus, P., Eds.; Springer: New York, NY, USA, 1985; pp. 267–268.

19. Wieder, H.H.; Clawson, A.R. Photo-electronic properties of $InAs_{0.07}Sb_{0.93}$ films. *Thin Solid Films* **1973**, *15*, 217–221. [CrossRef]

20. Miyoshi, H.; Horikoshi, Y. Substrate lattice constant effect on the miscibility gap of MBE grown InAsSb. *J. Cryst. Growth* **2001**, *227*, 571–576. [CrossRef]

21. Chou, C.Y.; Torfi, A.; Wang, W.I. Improvement of GaAsSb alloys on InP grown by molecular beam epitaxy with substrate tilting. *J. Appl. Phys.* **2013**, *114*, 153111. [CrossRef]

22. Gao, X.; Wei, Z.; Zhao, F.; Yang, Y.; Chen, R.; Fang, X.; Tang, J.; Fang, D.; Wang, D.; Li, R. Investigation of localized states in GaAsSb epilayers grown by molecular beam epitaxy. *Sci. Rep.* **2016**, *6*, 29112. [CrossRef] [PubMed]

23. Garbuzov, D.; Martinelli, R.; Lee, H.; Menna, R.; York, P.; DiMarco, L.; Harvey, M.; Matarese, R.; Narayan, S.; Connolly, J. 4 W quasi-continuous-wave output power from 2μm AlGaAsSb/InGaAsSb single-quantum-well broadened waveguide laser diodes. *Appl. Phys. Lett.* **1997**, *70*, 2931–2933. [CrossRef]

24. Karouta, F.; Mani, H.; Bhan, J.; Hua, F.J.; Joullie, A. Croissance par épitaxie en phase liquide et caractérisation d'alliages $Ga_{1-x}In_xAs_ySb_{1-y}$ à paramètre de maille accordé sur celui de GaSb. *Revue Phys. Appl.* **1987**, *22*, 1459–1467. [CrossRef]

25. Craig, A.; Jain, M.; Wicks, G.; Golding, T.; Hossain, K.; McEwan, K.; Howle, C.; Percy, B.; Marshall, A. Short-wave infrared barriode detectors using InGaAsSb absorption material lattice matched to GaSb. *Appl. Phys. Lett.* **2015**, *106*, 201103. [CrossRef]

26. Adachi, S. Band gaps and refractive indices of AlGaAsSb, GaInAsSb, and InPAsSb: Key properties for a variety of the 2~4μm optoelectronic device applications. *J. Appl. Phys.* **1987**, *61*, 4869–4876. [CrossRef]

27. Ait Kaci, H.; Boukredimi, D.; Mebarki, M. Band discontinuities of perfectly lattice-matched GaSb(n)/GaAlAsSb(p)/GaSb(p) double heterojunction. *Phys. Stat. Sol.* **1997**, *163*, 101–106. [CrossRef]

28. Jasik, A.; Kubacka-Traczyk, J.; Regiński, K.; Sankowska, I.; Jakieła, R.; Wawro, A.; Kaniewski, J. Method of determination of AlGaAsSb layer composition in molecular beam epitaxy processes with regard to unintentional as incorporation. *J. Appl. Phys.* **2011**, *110*, 073509. [CrossRef]

29. Gilliland, G.D. Photoluminescence spectroscopy of crystalline semiconductors. *Mater. Sci. Eng. R.* **1997**, *18*, 99–399. [CrossRef]

30. Baldereschi, A.; Lipari, N.C. Energy levels of direct excitons in semiconductors with degenerate bands. *Phys. Rev. B* **1971**, *3*, 439. [CrossRef]

31. Johnson, E.J.; Fan, H.Y. Impurity and exciton effects on the infrared absorption edges of III-V compounds. *Phys. Rev.* **1965**, *139*, A1991. [CrossRef]

32. Johnson, E.J. Absorption near the fundamental edge. *Semicond. Semimet.* **1967**, *3*, 153–258.

33. Lee, M.; Nicholas, D.; Singer, K.; Hamilton, B. A photoluminescence and Hall-effect study of GaSb grown by molecular-beam epitaxy. *J. Appl. Phys.* **1986**, *59*, 2895–2900. [CrossRef]

34. Yano, M.; Suzuki, Y.; Ishii, T.; Matsushima, Y.; Kimata, M. Molecular beam epitaxy of GaSb and $GaSb_xAs_{1-x}$. *Jpn. J. Appl. Phys.* **1978**, *17*, 2091. [CrossRef]

35. Gotoh, H.; Sasamoto, K.; Kuroda, S.; Yamamoto, T.; Tamamura, K.; Fukushima, M.; Kimata, M. S-doping of MBE-GaSb with H_2S gas. *Jpn. J. Appl. Phys.* **1981**, *20*, L893. [CrossRef]

36. Bignazzi, A.; Grilli, E.; Guzzi, M.; Radice, M.; Bosacchi, A.; Franchi, S.; Magnanini, R. Low temperature photoluminescence of tellurium-doped GaSb grown by molecular beam epitaxy. *J. Cryst. Growth* **1996**, *169*, 450–456. [CrossRef]

37. Georgitse, E.; Gutzuleac, L.; Mikhelake, A.; Postolachi, I.; Yuldashev, S.U.; Kang, T. Photoluminescence features of GaSb doped by Fe. *J. Lumin.* **2014**, *1*, 1–6. [CrossRef]

38. Blum, O.; Klem, J.F. Characteristics of GaAsSb single-quantum-well-lasers emitting near 1.3 μm. *IEEE Photonics Technol. Lett.* **2000**, *12*, 7773. [CrossRef]

39. Sakaki, H.; Chang, L.; Ludeke, R.; Chang, C.A.; Sai-Halasz, G.; Esaki, L. $In_{1-x}Ga_xAs$-$GaSb_{1-y}As_y$ heterojunctions by molecular beam epitaxy. *Appl. Phys. Lett.* **1977**, *31*, 211–213. [CrossRef]

40. Chang, C.A.; Ludeke, R.; Chang, L.; Esaki, L. Molecular-beam epitaxy(MBE) of $In_{1-x}Ga_xAs$ and $GaSb_{1-y}As_y$. *Appl. Phys. Lett.* **1977**, *31*, 759–761. [CrossRef]

41. Waho, T.; Ogawa, S.; Maruyama, S. $GaAs_{1-x}Sb_x$(0.3 < x < 0.9) grown by molecular beam epitaxy. *Jpn. J. Appl. Phys.* **1977**, *16*, 1875. [CrossRef]

42. Nahory, R.; Pollack, M.; DeWinter, J.; Williams, K. Growth and properties of liquid-phase epitaxial $GaAs_{1-x}Sb_x$. *J. Appl. Phys.* **1977**, *48*, 1607–1614. [CrossRef]

43. Cohen, R.; Cherng, M.; Benner, R.; Stringfellow, G. Raman and photoluminescence spectra of $GaAs_{1-x}Sb_x$. *J. Appl. Phys.* **1985**, *57*, 4817–4819. [CrossRef]

44. Merkel, K.; Bright, V.; Marciniak, M.; Cerny, C.; Manasreh, M. Temperature dependence of the direct band gap energy and donor-acceptor transition energies in Be-doped GaAsSb lattice matched to InP. *Appl. Phys. Lett.* **1994**, *65*, 2442–2444. [CrossRef]

45.　Castano, J.L.; Piqueras, J. Photoluminescence and doping in liquid phase epitaxial GaAs$_{1-x}$Sb$_x$. *J. Appl. Phys.* **1983**, *54*, 3422–3426. [CrossRef]

46.　Lukic-Zrnic, R.; Gorman, B.; Cottier, R.; Golding, T.; Littler, C.; Norman, A. Temperature dependence of the band gap of GaAsSb epilayers. *J. Appl. Phys.* **2002**, *92*, 6939–6941. [CrossRef]

47.　Nishino, F.; Takei, T.; Kato, A.; Jinbo, Y.; Uchitomi, N. Optical characterization of heavily Sn-Doped GaAs$_{1-x}$Sb$_x$ epilayers grown by molecular beam epitaxy on (001) GaAs substrates. *Jpn. J. Appl. Phys.* **2005**, *44*, 705. [CrossRef]

48.　Hsu, H.; Huang, J.; Huang, Y.; Lin, Y.; Lin, H.; Tiong, K. Optical study of GaAs$_{1-x}$Sb$_x$ layers grown on GaAs substrates by gas-source molecular beam epitaxy. *Mater. Chem. Phys.* **2010**, *124*, 558–562. [CrossRef]

49.　Qiu, W.; Wang, X.; Chen, P.; Li, N.; Lu, W. Optical spin polarization and Hanle effect in GaAsSb: Temperature dependence. *Appl. Phys. Lett.* **2014**, *105*. [CrossRef]

50.　Gao, X.; Wei, Z.; Fang, X.; Tang, J.; Fang, D.; Wang, D.; Chu, X.; Li, J.; Ma, X.; Wang, X. Effect of rapid thermal annealing on the optical properties of GaAsSb alloys. *Appl. Opt.* **2017**, *7*, 1971–1979. [CrossRef]

51.　Papis, E.; Piotrowska, A.; Kamińska, E.; Gołaszewska, K.; Kruszka, R.; Piotrowski, T.; Rzodkiewicz, W.; Szade, J.; Winiarski, A.; Wawro, A. Sulphur passivation of GaSb, InGaAsSb and AlGaAsSb surfaces. *Phys. Stat. Sol.* **2007**, *4*, 1448–1453. [CrossRef]

52.　Liu, Z.Y.; Kuech, T.F.; Saulys, D.A. A comparative study of GaSb(100) surface passivation by aqueous and nonaqueous solutions. *Appl. Phys. Lett.* **2003**, *83*, 2587–2589. [CrossRef]

53.　Banerjee, K.; Ghosh, S.; Plis, E.; Krishna, S. Study of short-and long-term effectiveness of ammonium sulfide as surface passivation for InAs/GaSb superlattices using X-ray photoelectron spectroscopy. *J. Electron. Mater.* **2010**, *39*, 2210–2214. [CrossRef]

54.　Bessolov, V.; Lebedev, M.; Novikov, E.; Tsarenkov, B. Sulfide passivation of III–V semiconductors: Kinetics of the photoelectrochemical reaction. *J. Vac. Sci. Technol. B* **1993**, *11*, 10–14. [CrossRef]

55.　Bessolov, V.N.; Lebedev, M.V. Chalcogenide passivation of III–V semiconductor surfaces. *Semiconductors* **1998**, *32*, 1141–1156. [CrossRef]

56.　Hu, J.; Odom, T.W.; Lieber, C.M. Chemistry and physics in one dimension: Synthesis and properties of nanowires and nanotubes. *Acc. Chem. Res.* **1999**, *32*, 435–445. [CrossRef]

57.　Lieber, C.M. One-dimensional nanostructures: Chemistry, physics & applications. *Solid State Commun.* **1998**, *107*, 607–616.

58.　Huang, M.H.; Mao, S.; Feick, H.; Yan, H.; Wu, Y.; Kind, H.; Weber, E.; Russo, R.; Yang, P. Room-temperature ultraviolet nanowire nanolasers. *Science* **2001**, *292*, 1897–1899. [CrossRef] [PubMed]

59.　Yang, P.; Yan, R.; Fardy, M. Semiconductor nanowire: What's next? *Nano Lett.* **2010**, *10*, 1529–1536. [CrossRef] [PubMed]

60.　Kim, H.; Lee, W.J.; Farrell, A.C.; Senanayake, P.; Huffaker, D.L. Monolithic InGaAs nanowire array lasers on silicon-on-insulator operating at room temperature. *arXiv* **2017**, arXiv:1701.02763. [PubMed]

61.　Saxena, D.; Mokkapati, S.; Parkinson, P.; Jiang, N.; Gao, Q.; Tan, H.H.; Jagadish, C. Optically pumped room-temperature GaAs nanowire lasers. *Nat. Photonics.* **2013**, *7*, 963–968. [CrossRef]

62.　Krogstrup, P.; Jørgensen, H.I.; Heiss, M.; Demichel, O.; Holm, J.V.; Aagesen, M.; Nygard, J.; Morral, A.F. Single-nanowire solar cells beyond the Shockley-Queisser limit. *Nat. Photonics* **2013**, *7*, 306–310. [CrossRef]

63.　Dai, X.; Zhang, S.; Wang, Z.; Adamo, G.; Liu, H.; Huang, Y.; Couteau, C.; Soci, C. GaAs/AlGaAs nanowire photodetector. *Nano Lett.* **2014**, *14*, 2688–2693. [CrossRef] [PubMed]

64.　Reimer, M.E.; Bulgarini, G.; Akopian, N.; Hocevar, M.; Bavinck, M.B.; Verheijen, M.A.; Bakkers, E.P.; Kouwenhoven, L.P.; Zwiller, V. Bright single-photon sources in bottom-up tailored nanowires. *Nat. Commun.* **2012**, *3*, 737. [CrossRef] [PubMed]

65.　Tomioka, K.; Yoshimura, M.; Fukui, T. A III–V nanowire channel on silicon for high-performance vertical transistors. *Nature* **2012**, *488*, 189. [CrossRef] [PubMed]

66.　Webb, J.L.; Persson, O.; Dick, K.A.; Thelander, C.; Timm, R.; Mikkelsen, A. High resolution scanning gate microscopy measurements on InAs/GaSb nanowire Esaki diode devices. *Nano Res.* **2014**, *7*, 877–887. [CrossRef]

67.　Dey, A.W.; Svensson, J.; Borg, B.M.; Ek, M.; Wernersson, L.E. Single InAs/GaSb nanowire low-power CMOS inverter. *Nano Lett.* **2012**, *12*, 5593–5597. [CrossRef] [PubMed]

68.　Borg, B.M.; Dick, K.A.; Ganjipour, B.; Pistol, M.E.; Wernersson, L.E.; Thelander, C. InAs/GaSb heterostructure nanowires for tunnel field-effect transistors. *Nano Lett.* **2010**, *10*, 4080–4085. [CrossRef] [PubMed]

69. Du, W.; Yang, X.; Pan, H.; Ji, X.; Ji, H.; Luo, S.; Zhang, X.; Wang, Z.; Yang, T. Controlled-Direction growth of planar inassb nanowires on si substrates without foreign catalysts. *Nano Lett.* **2016**, *16*, 877–882. [CrossRef] [PubMed]

70. Yang, Z.X.; Han, N.; Fang, M.; Lin, H.; Cheung, H.Y.; Yip, S.; Wang, E.J.; Hung, T.; Wong, C.Y.; Ho, J.C. Surfactant-assisted chemical vapour deposition of high-performance small-diameter GaSb nanowires. *Nat. Commun.* **2014**, *5*, 5249. [CrossRef] [PubMed]

71. Chin, A.; Vaddiraju, S.; Maslov, A.; Ning, C.; Sunkara, M.; Meyyappan, M. Near-infrared semiconductor subwavelength-wire lasers. *Appl. Phys. Lett.* **2006**, *88*. [CrossRef]

72. Calarco, R.; Marso, M.; Richter, T.; Aykanat, A.I.; Meijers, R.; vd Hart, A.; Stoica, T.; Lüth, H. Size-dependent photoconductivity in MBE-grown GaN-nanowires. *Nano Lett.* **2005**, *5*, 981–984. [CrossRef] [PubMed]

73. Kang, J.H.; Cohen, Y.; Ronen, Y.; Heiblum, M.; Buczko, R.; Kacman, P.; Popovitz-Biro, R.; Shtrikman, H. Crystal structure and transport in merged InAs nanowires MBE grown on (001) InAs. *Nano Lett.* **2013**, *13*, 5190–5196. [CrossRef] [PubMed]

74. Thelander, C.; Caroff, P.; Plissard, S.; Dick, K.A. Electrical properties of InAs$_{1-x}$Sb$_x$ and InSb nanowires grown by molecular beam epitaxy. *Appl. Phys. Lett.* **2012**, *100*, 232105. [CrossRef]

75. Xu, H.; Wang, Y.; Guo, Y.; Liao, Z.; Gao, Q.; Tan, H.H.; Jagadish, C.; Zou, J. Defect-free<110> zinc-blende structured InAs nanowires catalyzed by palladium. *Nano Lett.* **2012**, *12*, 5744–5749. [CrossRef] [PubMed]

76. Dubrovskii, V.G. Influence of the group V element on the chemical potential and crystal structure of Au-catalyzed III–V nanowires. *Appl. Phys. Lett.* **2014**, *104*, 053110. [CrossRef]

77. Krogstrup, P.; Curiotto, S.; Johnson, E.; Aagesen, M.; Nygård, J.; Chatain, D. Impact of the liquid phase shape on the structure of III–V nanowires. *Phys. Rev. Lett.* **2011**, *106*, 125505. [CrossRef] [PubMed]

78. Krogstrup, P.; Yamasaki, J.; Sørensen, C.B.; Johnson, E.; Wagner, J.B.; Pennington, R.; Aagesen, M.; Tanaka, N.; Nygård, J. Junctions in axial III–V heterostructure nanowires obtained via an interchange of group III elements. *Nano Lett.* **2009**, *9*, 3689–3693. [CrossRef] [PubMed]

79. Plissard, S.; Dick, K.; Wallart, X.; Caroff, P. Gold-free GaAs/GaAsSb heterostructure nanowires grown on silicon. *Appl. Phys. Lett.* **2010**, *96*. [CrossRef]

80. Ren, D.; Dheeraj, D.L.; Jin, C.; Nilsen, J.S.; Huh, J.; Reinertsen, J.F.; Munshi, A.M.; Gustafsson, A.; van Helvoort, A.T.; Weman, H. New insights into the origins of Sb-induced effects on self-catalyzed GaAsSb nanowire arrays. *Nano Lett.* **2016**, *16*, 1201–1209. [CrossRef] [PubMed]

81. Yu, X.; Li, L.; Wang, H.; Xiao, J.; Shen, C.; Pan, D.; Zhao, J. Two-step fabrication of self-catalyzed Ga-based semiconductor nanowires on Si by molecular-beam epitaxy. *Nanoscale* **2016**, *8*, 10615–10621. [CrossRef] [PubMed]

82. Holm, J.V.; Jørgensen, H.I.; Krogstrup, P.; Nygård, J.; Liu, H.; Aagesen, M. Surface-passivated GaAsP single-nanowire solar cells exceeding 10% efficiency grown on silicon. *Nat. Commun.* **2013**, *4*, 1498. [CrossRef] [PubMed]

83. Gorji Ghalamestani, S.; Ek, M.; Ganjipour, B.; Thelander, C.; Johansson, J.; Caroff, P.; Dick, K.A. Demonstration of defect-free and composition tunable Ga$_x$In$_{1-x}$Sb nanowires. *Nano Lett.* **2012**, *12*, 4914–4919. [CrossRef] [PubMed]

84. Svensson, J.; Anttu, N.; Vainorius, N.; Borg, B.M.; Wernersson, L.E. Diameter-dependent photocurrent in InAsSb nanowire infrared photodetectors. *Nano Lett.* **2013**, *13*, 1380–1385. [CrossRef] [PubMed]

85. Alarcón-Lladó, E.; Conesa-Boj, S.; Wallart, X.; Caroff, P.; Morral, A.F. Raman spectroscopy of self-catalyzed GaAs$_{1-x}$Sb$_x$ nanowires grown on silicon. *Nanotechnology* **2013**, *24*, 405707. [CrossRef] [PubMed]

86. Todorovic, J.; Kauko, H.; Ahtapodov, L.; Moses, A.; Olk, P.; Dheeraj, D.; Fimland, B.; Weman, H.; Van Helvoort, A. The effects of Sb concentration variation on the optical properties of GaAsSb/GaAs heterostructured nanowires. *Semicond. Sci. Technol.* **2013**, *28*, 115004. [CrossRef]

87. Senichev, A.V.; Talalaev, V.G.; Shtrom, I.V.; Blumtritt, H.; Cirlin, G.E.; Schilling, J.; Lienau, C.; Werner, P. Nanospectroscopic imaging of twinning superlattices in an individual GaAs/AlGaAs core-shell nanowire. *ACS Photonics* **2014**, *1*, 1099–1106. [CrossRef]

88. Dheeraj, D.L.; Patriarche, G.; Zhou, H.; Hoang, T.B.; Moses, A.F.; Grønsberg, S.; van Helvoort, A.T.; Fimland, B.O.; Weman, H. Growth and characterization of wurtzite GaAs nanowires with defect-free zinc blende GaAsSb inserts. *Nano Lett.* **2008**, *8*, 4459–4463. [CrossRef] [PubMed]

89. Conesa-Boj, S.; Kriegner, D.; Han, X.L.; Plissard, S.b.; Wallart, X.; Stangl, J.; Morral, A.F.; Caroff, P. Gold-Free ternary III-V antimonide nanowire arrays on silicon: Twin-free down to the first bilayer. *Nano Lett.* **2013**, *14*, 326–332. [CrossRef] [PubMed]

90. Munshi, A.M.; Dheeraj, D.L.; Todorovic, J.; van Helvoort, A.T.; Weman, H.; Fimland, B.O. Crystal phase engineering in self-catalyzed GaAs and GaAs/GaAsSb nanowires grown on Si (111). *J. Cryst. Growth* **2013**, *372*, 163–169. [CrossRef]

91. Baranowski, M.; Syperek, M.; Kudrawiec, R.; Misiewicz, J.; Gupta, J.; Wu, X.; Wang, R. Carrier dynamics between delocalized and localized states in type-II GaAsSb/GaAs quantum wells. *Appl. Phys. Lett.* **2011**, *98*, 061910. [CrossRef]

92. Lin, W.H.; Wang, K.W.; Lin, S.Y.; Wu, M.C. Temperature-dependent photoluminescence and carrier dynamics of standard and coupled type-II GaSb/GaAs quantum rings. *J. Cryst. Growth* **2013**, *378*, 426–429. [CrossRef]

93. Andreev, V.; Sorokina, S.; Timoshina, N.K.; Khvostikov, V.; Shvarts, M. Solar cells based on gallium antimonide. *Semiconductors* **2009**, *43*, 668–671. [CrossRef]

94. Jiang, Y.; Li, L.; Yang, R.Q.; Gupta, J.A.; Aers, G.C.; Dupont, E.; Baribeau, J.M.; Wu, X.; Johnson, M.B. Type-I interband cascade lasers near 3.2μm. *Appl. Phys. Lett.* **2015**, *106*, 041117. [CrossRef]

95. Mou, S.; Petschke, A.; Lou, Q.; Chuang, S.L.; Li, J.V.; Hill, C.J. Midinfrared InAs/GaSb type-II superlattice interband tunneling photodetectors. *Appl. Phys. Lett.* **2008**, *92*, 153505. [CrossRef]

96. Kujala, J.; Segercrantz, N.; Tuomisto, F.; Slotte, J. Native point defects in GaSb. *J. Appl. Phys.* **2014**, *116*, 143508. [CrossRef]

97. Tahini, H.; Chroneos, A.; Murphy, S.; Schwingenschlögl, U.; Grimes, R. Vacancies and defect levels in III–V semiconductors. *J. Appl. Phys.* **2013**, *114*, 063517. [CrossRef]

98. Huh, J.; Yun, H.; Kim, D.C.; Munshi, A.M.; Dheeraj, D.L.; Kauko, H.; van Helvoort, A.T.; Lee, S.; Fimland, B.O.; Weman, H. Rectifying single GaAsSb nanowire devices based on self-induced compositional gradients. *Nano Lett.* **2015**, *15*, 3709–3715. [CrossRef] [PubMed]

99. Lei, W.; Gu, R.; Antoszewski, J.; Dell, J.; Faraone, L. GaSb: A new alternative substrate for epitaxial growth of HgCdTe. *J. Electron. Mater.* **2014**, *43*, 2788–2794. [CrossRef]

100. Lei, W.; Gu, R.; Antoszewski, J.; Dell, J.; Neusser, G.; Sieger, M.; Mizaikoff, B.; Faraone, L. MBE growth of mid-wave infrared HgCdTe layers on GaSb alternative substrates. *J. Electron. Mater.* **2015**, *44*, 3180. [CrossRef]

101. Gu, R.; Antoszewski, J.; Lei, W. MBE growth of HgCdTe on GaSb substrates for application in next generation infrared detectors. *J. Cryst. Growth* **2017**, *468*, 216–219. [CrossRef]

102. Xia, F.; Wang, H.; Xiao, D.; Dubey, M. Two-dimensional material nanophotonics. *Nat. Photonics* **2014**, *8*, 899–907. [CrossRef]

103. Mak, K.F.; He, K.; Shan, J.; Heinz, T.F. Control of valley polarization in monolayer MoS_2 by optical helicity. *Nat. Nanotechnol.* **2012**, *7*, 494–498. [CrossRef] [PubMed]

104. Al Balushi, Z.Y.; Wang, K.; Ghosh, R.K.; Vilá, R.A.; Eichfeld, S.M.; Caldwell, J.D.; Qin, X.; Lin, Y.C.; DeSario, P.A.; Stone, G. Two-dimensional gallium nitride realized via graphene encapsulation. *Nat. Mater.* **2016**, *15*, 1166–1171. [CrossRef] [PubMed]

105. Zhang, S.; Yan, Z.; Li, Y.; Chen, Z.; Zeng, H. Atomically thin arsenene and antimonene: Semimetal-semiconductor and indirect-direct band-gap transitions. *Angew. Chem.* **2015**, *127*, 3155–3158. [CrossRef]

106. Zhuang, H.L.; Singh, A.K.; Hennig, R.G. Computational discovery of single-layer III–V materials. *Phys. Rev. B* **2013**, *87*, 165415. [CrossRef]

107. Singh, A.K.; Zhuang, H.L.; Hennig, R.G. Ab initio synthesis of single-layer III–V materials. *Phys. Rev. B* **2014**, *89*, 245431. [CrossRef]

108. Crisostomo, C.P.; Yao, L.Z.; Huang, Z.Q.; Hsu, C.H.; Chuang, F.C.; Lin, H.; Albao, M.A.; Bansil, A. Robust large gap two-dimensional topological insulators in hydrogenated III–V buckled honeycombs. *Nano Lett.* **2015**, *15*, 6568–6574. [CrossRef] [PubMed]